ChemPubSoc Europe

DOI: 10.1002/open.201800243

Open Access ChemistryOPEN Full Papers

Metal-Bonded Redox-Active Triarylamines and Their Interactions: Synthesis, Structure, and Redox Properties of Paddle-Wheel Copper Complexes

Oluseun Akintola, Michael Böhme, Manfred Rudolph, Axel Buchholz, Helmar Görls, and Winfried Plass*[a]

Four new triphenylamine ligands with different substituents in the *para* position and their corresponding copper(II) complexes are reported. This study includes their structural, spectroscopic, magnetic, and electrochemical properties. The complexes possess a dinuclear copper(II) paddle-wheel core, a building unit that is also common in metal-organic frameworks. Electrochemical measurements demonstrate that the triphenylamine ligands and the corresponding complexes are susceptible to oxidation, resulting in the formation of stable radical cations. The square-wave voltammograms observed for the complexes are similar to those of the ligands, except for a slight shift in potential. Square-wave voltammetry data show that, in the complexes, these oxidations can be described as individual one-electron processes centered on the coordinated ligands. Spectroelectrochemistry reveals that, during the oxidation of the complexes, no difference can be detected for the spectra of successively oxidized species. For the absorption bands of the oxidized species of the ligands and complexes, only a slight shift is observed. ESR spectra for the chemically oxidized complexes indicate ligand-centered radicals. The copper ions of the paddle-wheel core are strongly antiferromagnetic coupled. DFT calculations for the fully oxidized complexes indicate a very weak ferromagnetic coupling between the copper ions and the ligand radicals, whereas a very weak antiferromagnetic coupling is found among the ligand radicals.

1. Introduction

Triphenylamine-based molecules and their derivatives are a class of compounds widely studied due to their importance for the design of electronic materials,[1] which is particularly related to their pronounced hole-transport ability.[2] This fact coupled with the relatively low ionization potentials of triarylamines has led to their extensive application in electroluminescent devices as well as in photovoltaic materials.[3] Triarylamines typically undergo oxidation with ease resulting in the formation of a stable triarylammonium radical cation,[4] the stability of which depends on whether a *para* substitution at the aromatic rings is present or not.[5] For the cases of triphenylamines with an unsubstituted *para* position, these radicals are known to undergo dimerization to give tetraphenylbenzidines in a well-known oxidative coupling process. However, for the substituted derivatives a reversible redox behavior is observed, which can be tuned by varying the substituents attached to the aromatic rings particularly at the *para* positions.[6] Moreover, the molecular framework of triarylamines is also known to possess structural flexibility, which when coupled together with bulky substituents can lead to distortion or rotation within its structure.[7]

The unique electronic character of the triphenylamine moiety has led to its incorporation into molecular frameworks. This allows for interesting combinations of electronic and photophysical properties leading to new materials with appealing characteristics.[8] In particular, transition metal complexes with triphenylamine-based ligands have been used to investigate the charge-transfer properties of mixed valence systems.[9] In the latter cases, the well-known dinuclear paddle-wheel motif $M_2(RCOO)_4$ was used in combination with carboxylate-functionalized triphenylamine ligands. Moreover, this paddle-wheel motif is a common building unit for microporous coordination polymers, the so-called metal-organic frameworks (MOFs).[10] The dinuclear paddle-wheel fragment found in copper(II) acetate,[11] which can be regarded as an archetype for such building units, has been extensively utilized in MOFs since the seminal report on HKUST-1.[12] Such copper-based MOF systems are attracting significant interest and have been intensively investigated towards their electronic structure and other properties as well as potential applications.[13] On the other hand, 4,4′,4′′-nitrilotribenzoic acid (H_3ntb), a carboxylate derivative of triphenylamine, has found extensive use as linker in the construction of MOFs.[14] The molecular properties of the ntb^{3-} linker result in characteristic redox- and photo-active behavior of the corresponding MOFs which has led to specific applications such as sensing, catalysis, and generation of

[a] Dr. O. Akintola, M. Böhme, Dr. M. Rudolph, Dr. A. Buchholz, Dr. H. Görls, Prof. Dr. W. Plass
Institut für Anorganische und Analytische Chemie
Friedrich-Schiller-Universität Jena
Humboldtstr. 8, 07743 Jena, Germany
E-mail: sekr.plass@uni-jena.de

Supporting information for this article is available on the WWW under https://doi.org/10.1002/open.201800243

nanoparticles for hydrogen storage.[15] In fact, MOFs containing redox-active linkers of different type have been recently addressed toward their electrochemical behavior[16] and it could be shown that this can be used to control the properties of the corresponding frameworks.[17] Moreover, the combination of ntb^{3-} with ditopic linkers has been employed in the coordination copolymerization approach leading to multicomponent MOFs with interesting architectures including pillared-layer frameworks.[18] In this context, it should also be mentioned that extended triphenylamine-based linkers with two nitrogen centers have been utilized in the construction of MOFs with unusual architectures and properties.[19] In addition, also the generation of MOFs based on a branched triphenylamine-derived linker with even four nitrogen centers has been described.[20]

In this contribution, we present molecular model systems for the interaction of the copper paddlewheel moiety with triphenylamine-based ligands. For this purpose, the synthesis and characterization of four complexes of the general formula $[Cu_2(L)_4(dmf)_2]$ with ligands derived from 4-(diphenylamino) benzoic acid is reported. Of particular interest here is the redox behavior of the triphenylamine moiety and its interaction with the dinuclear core. This is investigated in view of the electronic and steric variation of the substituent at the *para* positions of the phenyl groups of the 4-(diphenylamino)benzoic acid ligand (R = H, Me, *t*-Bu, and OMe). To this end, electrochemical, structural, and magnetic properties are reported and complemented by theoretical calculations.

2. Results and Discussion

2.1. Synthesis and Characterization

The ligand 4-(diphenylamino)benzoic acid (Haba, **1**) was obtained in a two-step synthetic route. In the first step, the formylation of triphenylamine was performed through the Vilsmeier–Haack reaction using phosphoryl chloride in dimethylformamide.[21] The resulting aldehyde was subsequently oxidized with $KMnO_4$ under alkaline conditions followed by acidification of the resultant potassium salt using concentrated aqueous HCl according to a modified published procedure for the 4,4′-(phenylazanediyl)dibenzoic acid (see Scheme 1).[22]

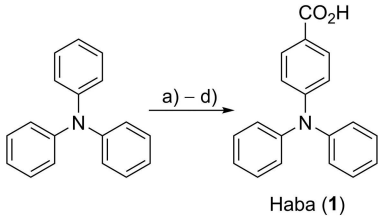

Scheme 1. Synthesis of 4-(diphenylamino)benzoic acid (Haba, **1**): a) $POCl_3$, dmf, 0 °C; b) reflux under N_2 for 22 h; c) K_2CO_3, $KMnO_4$, acetone, reflux, 12 h; d) HCl.

On the other hand, the ligands with substituents at the *para* position of the two phenyl rings, namely 4-(bis(4-methylphenyl) amino)benzoic acid (Haba-Me, **2**), 4-(bis(4-*tert*-butylphenyl) amino)benzoic acid (Haba-tBu, **3**), and 4-(bis(4-methoxyphenyl) amino)benzoic acid (Haba-OMe, **4**) were obtained via a Buchwald–Hartwig palladium catalyzed coupling reaction. For each ligand its bromophenyl precursor (4-bromotoluene, 4-*tert*-butylbromobenzene, and 4-bromoanisole for **2**, **3**, and **4**, respectively) was combined with methyl 4-aminobenzoate while using Cs_2CO_3 as base. The resultant ester was subsequently subjected to alkaline hydrolysis followed by acidification with concentrated aqueous HCl (see Scheme 2).[23]

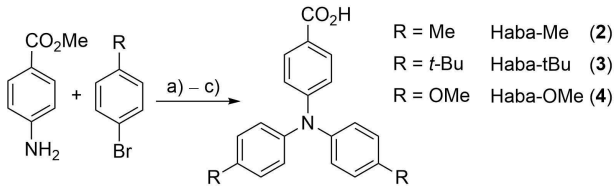

Scheme 2. Preparation scheme for **2**–**4**: a) Pd/P(*t*-Bu)$_3$; Cs_2CO_3, toluene, 110 °C, 5–7 d; b) KOH, MeOH, reflux; c) HCl.

The synthesis of the copper complex $[Cu_2(aba)_4(dmf)_2]$ (**5**) was performed by a solvothermal process in dmf using copper (II) nitrate. The use of acetonitrile was avoided due to its reported tendency to aid oxidation of triphenylamines in the presence of copper(II) ions, which in turn leads to the formation of the benzidine derivative.[24] An alternative route to synthesize **5** is given by reacting the ligand and copper(II) nitrate in ethanol. By layering the resultant solution with dmf it was possible to obtain green crystals of **5** within a period of 2–3 weeks. Both routes led to good quality crystals suitable for X-ray crystallographic studies. Similarly also the complex $[Cu_2(aba\text{-}Me)_4(dmf)_2]$ (**6**) was prepared via the solvothermal route, which yielded a light green solution. To reduce the solubility of the product methanol was slowly layered on top of the obtained solution, which was allowed to stand for a few hours, upon which a light green precipitate formed. Additional material as green block crystals was obtained from the filtrate after it was left standing for slow evaporation. An alternative route to **6** was established by heating a solution of both the ligand and copper (II) nitrate in dmf at 110 °C for 30 min. Subsequent cooling of the reaction solution and allowing it to stand for a few days resulted in the formation of micro-crystalline product, which was unfortunately not suitable for X-ray crystallography. This latter route of simply refluxing a mixture of the metal salt and ligand in dmf was successfully used in the synthesis of the complex $[Cu_2(aba\text{-}tBu)_4(dmf)_2]$ (**7**), yielding crystalline material also suitable for X-ray structure determination. For the complex $[Cu_2(aba\text{-}OMe)_4(dmf)_2]$ (**8**) again the solvothermal route similar to **5** and **6** was employed for the synthesis. However, this only led to the formation of dark green micro crystals which were not suitable for single crystal X-ray studies. Nevertheless, crystals suitable for X-ray studies were obtained by stirring both ligand and metal salt in dmf for about 20 min followed by

slowly layering methanol on top of this solution. Both solvents were then allowed to slowly evaporate over 4 weeks to yield green crystals of **8**.

The composition of the obtained bulk material for compounds **5**–**8** was analyzed by elemental and thermogravimetric analysis, which revealed the presence of varying amounts of different solvent molecules of crystallization. The corresponding data is given in Figure S1 and Table S1.

2.2. X-ray Crystal Structures

The crystallographic characterization reveals that all four complexes **5**–**8** crystallize in the triclinic space group $P\bar{1}$ (see Table S2 for details). The molecular structure of **5** depicted in Figure 1 is representative of the other isostructural complexes

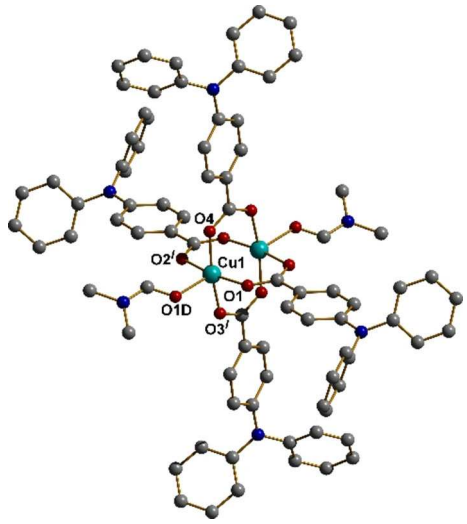

Figure 1. Molecular structure of **5** with hydrogen atoms omitted for clarity.

6–**8** and shows that a dimeric paddle-wheel arrangement is adopted. As the center of the paddle-wheel dimers, for the crystal structures of all complexes, is situated on a crystallographic inversion center, only half of the complex molecules are within the asymmetric units. A comparison of the selected bond lengths in all four complexes is summarized in Table S3 and additional representations of the molecular structures of **6**–**8** including full labeling are given in Figures S2–S5.

The molecular structure consists of four bridging carboxylate ligands and two axial coordinated dmf ligands at the two copper(II) ions as shown in Figure 1. Each copper ion is coordinated by four oxygen atoms from different carboxylate groups in the equatorial plane with distances at around 196 pm. The carboxylate C–O bond lengths are close to 126 pm, while the Cu···Cu distances are at about 260 pm. Together with the oxygen donor of the coordinating dmf molecule in the axial position at a distance of about 216 pm (Cu1–O1D, see Table S3) this leads to a square pyramidal coordination geometry. For all complexes the copper centers are displaced by about 18 pm from the basal [O_4] plane towards the dmf oxygen donor atom.

The phenyl rings of the triphenylamine moieties in the complexes are twisted out of the plane of the central nitrogen atom (cf. Figure S6). This is enforced by repulsion between the phenyl rings and packing effects, leading to corresponding angles Φ within the range from 21 to 65° (see Table S4). Moreover, also the planarity at the central nitrogen atom varies considerably (average distance of the nitrogen atom from the plane: 3.4, 5.9, 7.1, and 13.9 pm for **5**, **6**, **7**, and **8**, respectively; cf. Table S4), which is most likely also indicative for electronic effects of the substituents at the *para* position, similar to what is observed for electrochemical properties and UV/vis spectra (vide infra). In contrast, the dihedral angle between the carboxylate group coordinating the central paddle-wheel unit and the connected phenyl group (see Figure S7) shows a considerably smaller variation within the range from 5.2 to 27.8°, consistent with an overall reduced influence of the above-mentioned effects. As expected the four nitrogen centers of the triphenylamine moieties show an almost rectangular planar arrangement with N···N distances of about 1160 pm along the edges with the largest variation observed for **8** (1088 and 1235 pm) while the diagonal distances are approximately 1647 pm (see Figure S8 and Table S5).[25]

Except for the crystal structure of complex **8** all the other three complexes **5**–**7** contain additional solvent molecules of crystallization. In the case of complex **6** one co-crystallized dmf molecule was found that is disordered over two crystallographic positions. The X-ray powder diffraction (XRPD) measurements on bulk material of complexes **6** and **8** is in agreement with the corresponding simulated patterns obtained from the single crystal X-ray measurements (see Figure S9). However, the situation is somewhat different for the complexes **5** and **7**, which both possess a rather large void space in the crystal structure. The disordered solvent molecules crystallized in these voids could not be located and have been treated using the SQUEEZE routine (see Experimental Section). Consequently, for the latter two complexes (**5** and **7**) differences between the experimental and simulated XRPD patterns are observed (see Figure S9). This can be attributed to corresponding structural changes related to solvent loss upon drying the bulk material or the possible presence of a second crystalline phase with the same molecular composition. Moreover, differences in intensities of individual reflections may also be due to orientation effects of the crystallites.

2.3. Magnetic Properties

The magnetic susceptibility data for the complexes **5**–**8** were obtained in the temperature range from 4 to 300 K. Figure 2 shows the representative data for complex **5** as temperature-dependent plot of $\chi_M T$ (for data **6**–**8** see Figure S10). The $\chi_M T$ values at 300 K for the four complexes **5**–**8** are about 0.46 $cm^3\,K\,mol^{-1}$, which is only slightly above half the spin-only value of 0.75 $cm^3\,K\,mol^{-1}$ expected for two independent copper (II) ions.[26] Upon lowering the temperature the $\chi_M T$ value

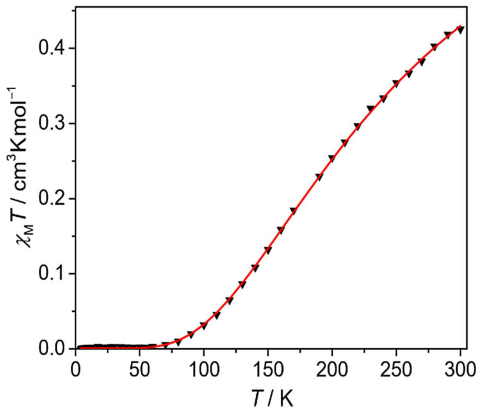

Figure 2. Temperature dependence of the magnetic susceptibility $\chi_M T$ for complex **5** measured at an applied field of 2 kOe. The solid red line represents the best fit.

decreases to very small values in all cases at a temperature of about 70 K indicating a diamagnetic ground state. Overall, this behavior is consistent with antiferromagnetic exchange coupling between the copper(II) centers of the paddle-wheel moiety.[27] The experimental data were fitted using the program PHI[28] applying the Heisenberg Hamiltonian $\hat{H} = -J\hat{S}_1\hat{S}_2$.The best fit is obtained for the parameters given in Table 1. The

Table 1. Parameters obtained from fitting the magnetic susceptibility data of **5**–**8** with corresponding data obtained from theoretical calculations (vide infra).

	g	J_{exp} [cm^{-1}]	J_{calcd} [cm^{-1}]
5	2.14	−321	−345
6	2.12	−295	−351
7	2.18	−330	−336, −346[a]
8	2.23	−320	−345

[a] The single-crystal structure of **7** contains a disorder for the dmf co-ligands at the copper centers.

resulting exchange coupling constants of the four complexes are virtually invariant with respect to the type of substituent present at the *para* positions of the phenyl groups of the triphenylamine ligand moieties.

To corroborate the experimental data and to gain further insight with respect to the coupling constants we have performed broken-symmetry DFT (BS-DFT) calculations for the complexes **5**–**8**. The corresponding results are included in Table 1 (for detailed data see Table S6). The BS-DFT calculations confirm the strong antiferromagnetic coupling between the copper centers of the paddle-wheel unit obtained by simulating the experimental data. These strong antiferromagnetic exchange interactions are a result of the congruent alignment of the square planar coordination environment of the two copper (II) centers in the complexes which are bridged by four aryl carboxylates. Nevertheless, the calculated coupling constants slightly overestimate the experimental values,[29] where the largest deviation is found for **6** ($J_{exp} = -295$ cm^{-1}; $J_{calcd} = -351$ cm^{-1}). Moreover, only a small variation within the calculated coupling constants can be found ($|J_{calcd}| = 336$–351 cm^{-1}) indicating a negligible electronic effect of the different substituents present in the ligand backbone. In fact, the observed variation based on the structural disorder of the dmf co-ligands in **7** is with 10 cm^{-1} (**7**(A): −336; **7**(B): −346 cm^{-1}) in the same range as the observed variation over all complexes **5**–**8**. Spin density plots for the high-spin and broken-symmetry state of the complexes **5**–**8** (see Figures S11–S14) show that the spin density in all complexes is primarily localized on the paddle-wheel core, i.e. in the $d^{x^2-y^2}$ magnetic orbitals of the copper(II) ions. This further supports the idea of negligible electronic effects of the *para* substituents at the triphenylamine moiety.

To further investigate the effect of the triphenylamine moieties and their attached *para* substituents on the exchange coupling within the dicopper core unit two additional structurally reduced models have been used for BS-DFT calculations. In the medium model (**5**^{M}–**8**^{M}) the *para* substituted phenyl groups at the bridging aminobenzoates have been replaced by methyl groups, whereas in the small model (**5**^{S}–**8**^{S}) the amine substituent at the bridging benzoates have been completely removed and replaced by hydrogen atoms. For both reduced models the structural parameters are based on the crystal structures of the complexes **5**–**8**. The corresponding results summarized in Tables S7 and S8 show that both reduced models can reproduce the strong antiferromagnetic coupling obtained from the calculations for the full complexes. Interestingly, the results from both reduced models differ with a mean value less than 3 cm^{-1} from the values obtained for the calculations based on the original structure of the complexes **5**–**8**, with two slightly larger deviations observed for **6**^{S} (6 cm^{-1}) and **8**^{S} (4 cm^{-1}). This further indicates that neither the substitution pattern at the triphenylamine moieties nor the amino groups as such at the bridging benzoate groups have a significant effect on the exchange coupling between the copper(II) centers of the paddle-wheel unit.

2.4. Electrochemical Properties

The cyclic voltammogram of ligand **1** is indicative for an irreversible process with a single peak in the anodic scan, corresponding to the oxidation of monomeric species to radical cations, which subsequently dimerize to form a tetraphenylbenzidine (TPB) dication.[30] In the following cathodic scan two reduction peaks were observed, which can be attributed to the reduction of the TPB dication to the monocation and then further to the neutral dimer (see Figure S15).[31] The same behavior was likewise seen for complex **5** and is consistent with reported triphenylamine systems that have an attached *para* substituent only at one of the phenyl rings.[32] The observed tendency to dimerize unfortunately hampered any further detailed studies on these systems.

For the analogous *para* substituted ligands **2**–**4** square-wave voltammetry measurements were carried out. The absence of the oxidative coupling reaction due to the occupied *para* positions allows for the observation of more detailed

features related to the electron-transfer process in these cases. The oxidation of the ligands **2**–**4** can be described in terms of single quasi-reversible one-electron oxidation steps. The underlying mechanism for the simulation of the recorded square-wave voltammetric data is given in Equations (1) and (2), where E° is the standard potential, k_s the heterogeneous rate constant, α the charge-transfer parameter, D the diffusion coefficient, and k_f the rate constant for the subsequent chemical reaction.

$$HL^+ + e^- \rightleftharpoons HL \ (E^\circ, k_s, \alpha, D) \quad (1)$$

$$HL^+ \rightarrow P \ (k_f) \quad (2)$$

The data obtained from simulation are summarized in Table 2. The reported standard potentials E° are assigned to the

Table 2. Experimental parameters from simulating square-wave voltammograms of the ligands **2**–**4**.

	2	**3**	**4**
R	Me	*t*-Bu	OMe
D [10^{-6} cm^2 s^{-1}]	8.5	6.9	7.8
E° [mV]	550	556	388
k_s [cm s^{-1}]	0.13	0.16	0.14
k_f [10^{-4} s^{-1}]	≈4	≈4	≈4

half-wave potentials derived from square-wave voltammetry. This assignment is justified by approximately equal diffusion coefficients of the oxidized and reduced species,[33] which was confirmed by cyclic voltammetric studies at a platinum disk electrode (Ø = 10 μm). Moreover, the charge-transfer parameter was assumed to be $\alpha = 0.5$, since varying this parameter over the range $0.45 \leq \alpha \leq 0.55$ has only a negligible small effect on the standard deviation between simulated and experimental curves. It should be noted that the k_f values reported in Table 2 not only minimize the difference between experimental and simulated square-wave voltammograms, but also the difference between experimental and simulated thin-layer cyclic voltammograms measured in the course of the spectroelectrochemical experiments (vide infra). A thorough analysis of the electrochemical data for the ligand systems **2**–**4** (see Figure S16) reveals that an error of 1 mV in the standard potential E° has approximately the same effect on the standard deviation as errors of about 0.3×10^{-6} cm^2 s^{-1} in the diffusion coefficient D and about 0.05 cm s^{-1} in the heterogeneous rate constant k_s, respectively. In fact, with respect to the estimated errors the heterogeneous rate constant is essentially the same for all ligands, i.e. $k_s \approx 0.15 \pm 0.05$ cm s^{-1}.

A comparison of the diffusion coefficients of the ligands **2**–**4** shows the expected trend with the bulky *tert*-butyl substituted ligand exhibiting the slowest diffusion followed by the methoxy and methyl analogues in that order. Similarly, the values of the standard potentials match the expected electronic trend given by the *para* substituents at the triphenylamine moiety.[34] The representative square-wave voltammograms of ligand **4** are displayed in Figure 3 and show good agreement between simulated and experimental data (for **2** and **3** see Figure S17).

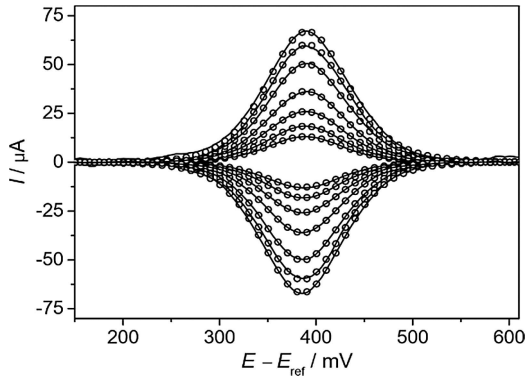

Figure 3. Square-wave voltammograms of the ligand **4** ($c = 1.95$ mM) in dichloromethane solution at square-wave frequencies of 25, 50, 100, 200, 400, 600, and 750 Hz. Open circles represent simulated and lines experimental data.

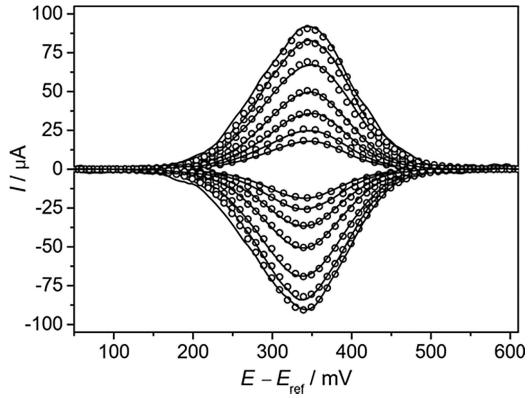

Figure 4. Square-wave voltammograms of the complex **8** ($c = 1.18$ mM) in dichloromethane solution at square-wave frequencies of 25, 50, 100, 200, 400, 600, and 750 Hz. Open circles represent simulated and lines experimental data.

The square-wave voltammograms recorded for the complexes **6**–**8** show a rather similar behavior as those observed for their corresponding ligands. In Figure 4 the square-wave voltammograms of **8** are depicted as a representative example (for **6** and **7** see Figure S18). The oxidation of the complexes **6**–**8** can be described according the underlying mechanism given in Equations (3)–(6), where E_i° are the standard potentials for the individual one-electron steps.

$$[Cu_2(aba\text{-}R)_4]^+ + e^- \rightleftharpoons [Cu_2(aba\text{-}R)_4] \ (E_1^\circ) \quad (3)$$

$$[Cu_2(aba\text{-}R)_4]^{2+} + e^- \rightleftharpoons [Cu_2(aba\text{-}R)_4]^+ \ (E_2^\circ) \quad (4)$$

$$[Cu_2(aba\text{-}R)_4]^{3+} + e^- \rightleftharpoons [Cu_2(aba\text{-}R)_4]^{2+} \ (E_3^\circ) \quad (5)$$

$$[Cu_2(aba\text{-}R)_4]^{4+} + e^- \rightleftharpoons [Cu_2(aba\text{-}R)_4]^{3+} \ (E_4^\circ) \quad (6)$$

Consistent with the data presented for the ligands also for the complexes the charge-transfer parameter α was supposed to be 0.5 for all four charge-transfer reactions. Moreover, it was further assumed that the diffusion coefficient D and the heterogeneous rate constant k_s are related to the particular

complex system and are independent of the charge of the individual species. The parameters obtained from simulation of the experimental square-wave voltammograms are presented in Table 3.

Table 3. Experimental parameters obtained from simulating square-wave voltammograms of the complexes **6**–**8**.

R	**6** Me	**7** *t*-Bu	**8** OMe
D [10^{-6} cm^2 s^{-1}]	4.8	3.2	4.0
E_1° [mV]	451	467	283
E_2° [mV]	497	503	329
E_3° [mV]	521	527	351
E_4° [mV]	558	562	389
k_s [cm s^{-1}]	0.170	0.110	0.150

Qualitatively the diffusion coefficients of the complexes are following the same trend as observed for the related ligands. Nevertheless, the absolute values are as expected smaller than those of the corresponding ligands. Moreover, the voltammograms are only dependent on the ligand present, rather than being indicative of a metal ion-centered process. The standard potentials observed for the complexes **6**–**8** show a slight shift which corresponds to the substitution pattern of the related ligand. The individual oxidation steps given in Equations (3) to (6) can be described as single one-electron processes despite the presence of four oxidizable centers. Such a behavior is theoretically expected if the interactions between the electrochemically active centers are negligibly small and the charge-transfer process is virtually reversible.[35] Simulation of the experimental data allowed determination of the separation between the standard potential of the four oxidation steps which are summarized in Table 4 and compared to the corresponding values expected for a simple entropy effect with ΔE_S.[36]

Table 4. Separations between the standard potential of individual one-electron processes for complexes **6**–**8** as compared with value expected from a solely entropy-related effect ΔE_S.

R	**6** Me	**7** *t*-Bu	**8** OMe	ΔE_S
E_2°–E_1° [mV]	46	36	46	25
E_3°–E_2° [mV]	24	24	22	21
E_4°–E_3° [mV]	37	35	38	25

An important observation to note is that experimental square-wave voltammograms are distinctly broader than expected from the pure entropy effect for a system containing four chemically identical oxidizable ligands. Moreover, this discrepancy also holds for the differences between the individual standard potentials of the four oxidation steps, for which significantly larger values are observed than those estimated from the presence of a solely entropy effect of four chemically equivalent oxidizable fragments in the system. Remarkably, the standard potential of the fourth oxidation step (Equation (6)) is close to the potential observed for the corresponding ligand (see Tables 2 and 3).

2.5. Spectroelectrochemistry

To further explore the electrochemical oxidation of the complexes **6**–**8** and to probe the electronic properties of oxidized species spectroelectrochemical investigations have been performed. In order to address this point we first performed spectroelectrochemical measurement for the corresponding ligands to examine their properties as a basis for the understanding of the related complexes. It has to be noted here that a general assumption is required for simulating electrochemical data recorded with an optically transparent thin-layer electrochemical (OTTLE) cell as used in our experiments. Generally, the theoretical model to simulate thin-layer cyclic voltammograms assumes a cell geometry for which one of the boundaries is a smooth optically transparent electrode, while the other being an optically transparent insulator. However, the experimental thin-layer cell consists of two optically transparent insulators having a platinum net electrode in between. Consequently, unlike in the case of the simulated cyclic voltammograms, the shape of the experimental ones does not only depend on diffusion processes occurring perpendicular to the electrode, but also on processes occurring within the meshes of the platinum net.

In Figure 5 the experimental and simulated thin-layer cyclic voltammograms for ligand **3** and complex **7** are depicted as representative examples (for ligands **2** and **4** as well as complexes **6** and **8** see Figure S19), indicating a suitable agreement and proving the validity of the assumption made to simulate the data (also cf. Table 2). In fact, it is obvious that the differences between both data sets are smaller for lower scan rates. This is consistent with the limiting condition that the shape of the thin-layer cyclic voltammograms becomes independent of the diffusion processes, if the scan rate and/or the cell thickness tends toward zero.

The UV/vis absorption spectra recorded for ligand **3** during the electrochemical forward and back ward scan are depicted as a representative example in Figure 6 (for **2** and **4** see Figure S20). A factor analysis of the spectra obtained for the three ligands during thin-layer cyclic voltammetry experiments revealed that only a single optically active species is produced in the forward scan, while in the backward scan this species is completely consumed, which is consistent with the observed quasi-reversible one-electron oxidation steps for the ligands in the square-wave voltammetry measurements. Consequently, it was possible to determine the UV/vis absorption spectra of the corresponding oxidized ligands which are depicted in Figure 7. The values of the molar extinction coefficients are based on the assumption that the optical path length of the thin-layer cell is exactly 0.2 mm. However, the uncertainty estimated for the absolute value is about 10%, despite the fact, that the reproducibility of the individual species spectra was distinctly better in a series of independent experiments.

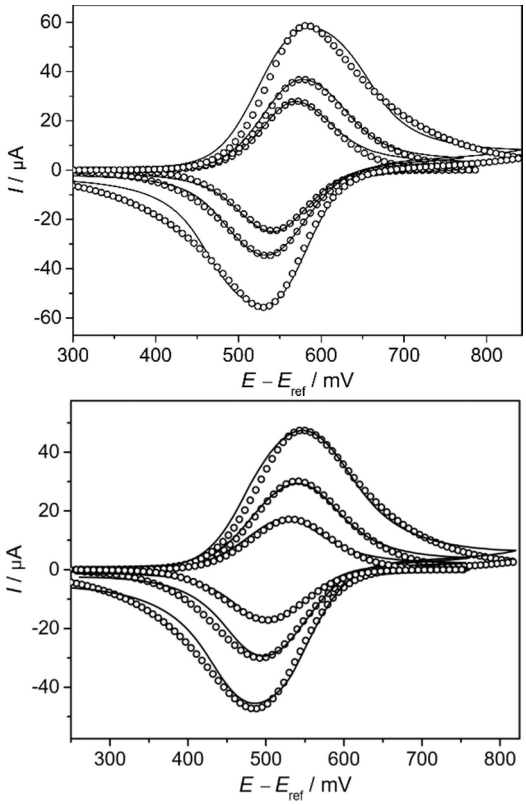

Figure 5. Thin-layer cyclic voltammograms of ligand **3** (top, $c = 2.40$ mM) and complex **7** (bottom, $c = 0.59$ mM) in dichloromethane solutions using scan rates of 1.25, 2.5, and 5 mV s^{-1}. Open circles represent simulated and lines experimental data.

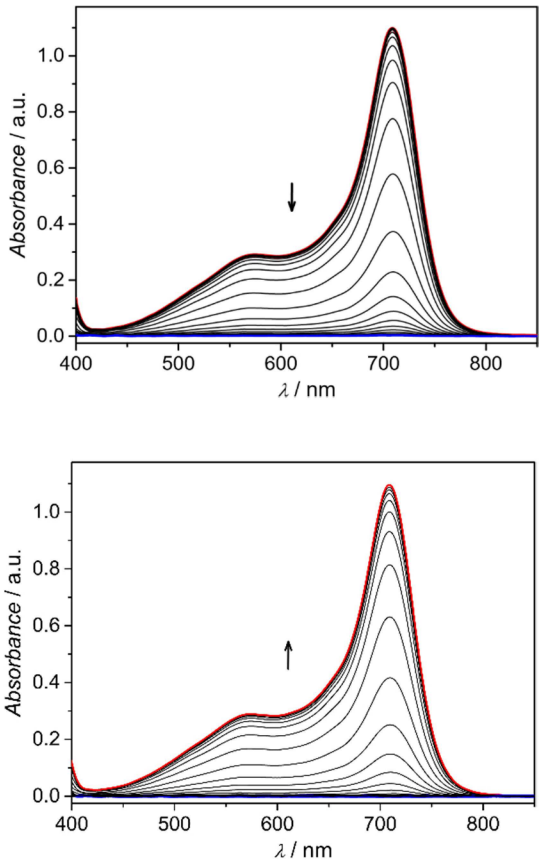

Figure 6. UV/vis spectra recorded during the electrochemical forward (top, blue to red line) and backward (bottom, red to blue line) scan for ligand **3** ($c = 2.40$ mM). The difference in potential between successive spectra is 20 mV.

The maxima in the observed UV/vis spectra of the oxidized ligands were found at 701, 711, and 784 nm for **2**, **3**, and **4**, respectively, which can be assigned as the HOMO→LUMO transitions, with both orbitals having π character. For all three oxidized ligands additional less intense bands at higher energies are observed (**2**: 570; **3**: 576; **4**: 544 and 584 nm), which is typical for triphenylamine systems with lower symmetry.[37] This shows a clear trend for the ligands that the lowest energy absorption is shifted toward higher wavelengths within the series of methyl (**2**), *tert*-butyl (**3**), and methoxy (**4**) substitution, which is consistent with the variation of the electronic properties of *para* substituents and also reflects the trend observed for the standard potentials (cf. Table 2). Moreover, the observed trend is also consistent with the values reported for the corresponding symmetrically substituted triphenylamines.[4,38] Interestingly, the extinction coefficient of the absorption maximum for the methoxy substitute ligand **4** is significantly larger than those observed for ligands **2** and **3**.

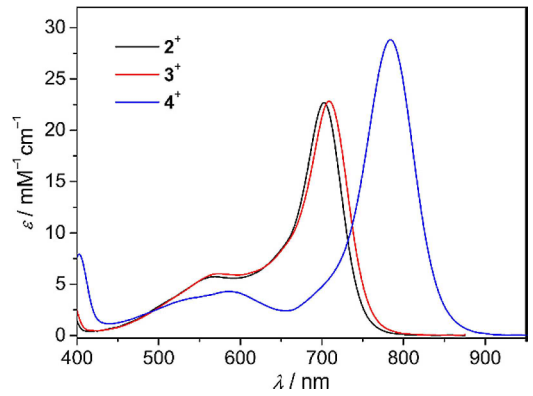

Figure 7. UV/vis spectra of the oxidized species for ligands **2** (black line), **3** (red line), and **4** (blue line) determined from spectroelectrochemical experiments.

Spectroelectrochemical investigations were also performed for the complexes **6**–**8** by recording UV/vis absorption spectra during the electrochemical forward and backward scan, which are shown for **7** as a representative example in Figure 8 (for **6** and **8** see Figure S21). As in the case of the ligands factor analysis of the spectra of the copper complexes reveals that only a single optically active species is produced in the forward scan of each thin-layer cyclic voltammetry experiment, which is consumed during the following backward scan. Therefore, the absorption spectra of the oxidized copper complexes can be extracted from the data, again assuming an idealized optical path length as in the ligand case. The obtained spectra of the complexes **6**–**8** are depicted in Figure 9.

For the absorption maxima of the complexes a similar basic trend as in the case of the corresponding ligands is observed,

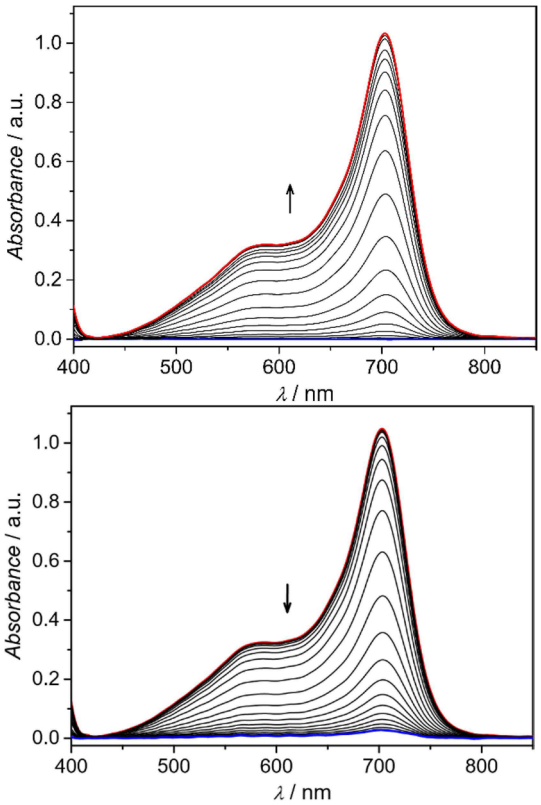

Figure 8. UV/vis spectra recorded during the electrochemical forward (top, blue to red line) and backward (bottom, red to blue line) scan for complex **7** ($c = 0.59$ mM). The difference in potential between successive spectra is 20 mV.

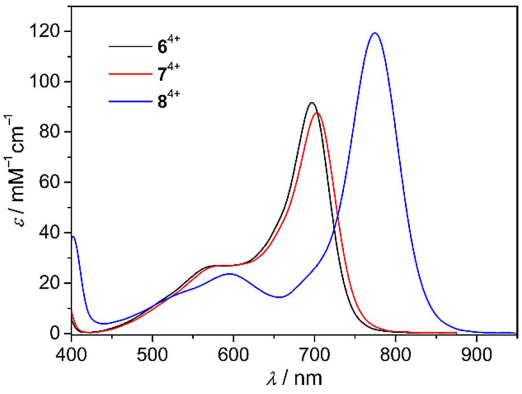

Figure 9. UV/vis spectra of the oxidized species of the complexes **6** (black line), **7** (red line), and **8** (blue line) determined from spectroelectrochemical experiments.

where again the highest wavelength is found for the methoxy derivative **8**. However, comparing the absorption maxima of the ligands and complexes a slight shift to lower wavelengths is observed for the complexes with about 5, 6, and 10 nm for **6**, **7**, and **8**, respectively (cf. Figures 7 and 9), indicative for only minor contributions of the copper paddle-wheel unit on the optical properties of the oxidized ligand moieties in the complexes. As in the case of the ligands the methoxy derivative shows the largest extinction coefficient for the absorption maximum. A comparison of the spectra obtained for the ligands and complexes reveals an approximately four-fold increase in the extinction coefficient (see Figure S22). Therefore, it is tempting to assume that the complex spectra can be viewed as a simple sum of four individual ligand spectra. This view is consistent with the fact that only one optically active species is generated during the oxidation of the complexes **6**–**8**. In fact, there is no indication for any difference in the spectra of the oxidized species obtained by successive oxidations steps, which means that all oxidized species $[Cu_2(aba\text{-}R)_4]^{n+}$ independent of their charge have the same spectra only related to the variation of the *para* substituents. This is further evidenced by the comparison of UV/vis spectra recorded at different potentials during the spectroelectrochemical oxidation, which are related to different molar fractions of the possible charged species. The latter can be concluded from the fact that the difference in standard potentials of the four oxidation processes cannot solely be related to the pure entropy term (cf. Table 4). Indeed, applying an appropriate scaling factor the spectra obtained for intermediate potentials can be superimposed with the spectrum of the fully oxidized complex cation (see Figure S23 for complex **6** as a representative case).

2.6. Chemical Oxidation of Ligands and Complexes

Chemical oxidation of the ligands and complexes was carried out with silver tetrafluoroborate as an oxidant in dichloromethane solution. It was observed that the methoxy derivatives **4** and **8** showed greatest ease in oxidation, for which it was possible to obtain the oxidized species upon addition of stoichiometric amounts of oxidant. This is consistent with the appreciably lower standard potential observed for **4** and **8** with respect to the other derivatives (see Tables 2 and 3). The corresponding UV/vis absorption spectra recorded for the chemically oxidized species of the ligand **4** and complex **8** are depicted in Figure 10. However, due to their higher standard potentials, the methyl (**2** and **6**) and *tert*-butyl (**3** and **7**) counterparts required an excess of oxidant to obtain the radical species. The corresponding UV/vis spectra of their chemically oxidized species depicted in Figure S24 are in full agreement with the data obtained from the spectroelectrochemical experiments (vide supra). It is interesting to note here that the oxidized species of all ligands and complexes did generally show a remarkable stability, as their spectra did not change appreciably over time for at least several days, particularly when care was taken to prevent solvent evaporation. This even holds for samples which were appropriately stored in contact to ambient atmosphere.

To further characterize the oxidized species derived from the ligands **2**–**4** and complexes **6**–**8** room temperature X-band ESR spectra were recorded. The radicals were obtained by treating solutions of the ligands and complexes in dichloromethane with an excess of silver tetrafluoroborate, upon which the solutions turned deep blue-violet to give the corresponding radicals. The ESR spectra recorded for the chemically oxidized

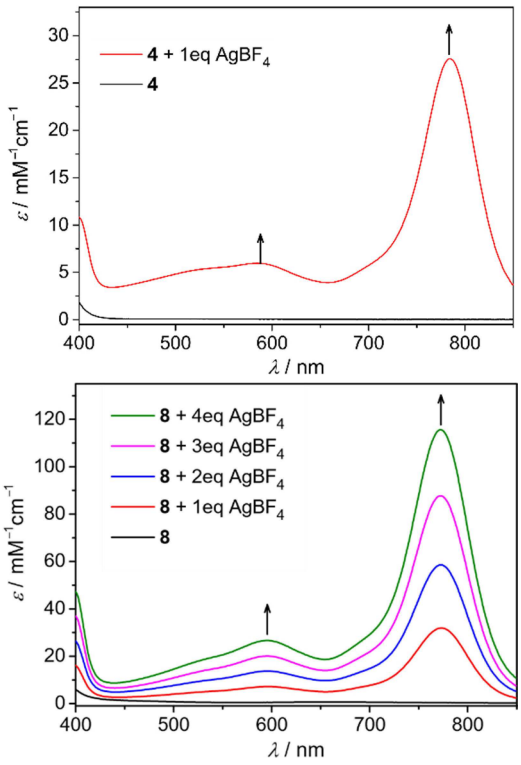

Figure 10. UV/vis spectra for the chemically oxidized species of ligand **4** (top) and complex **8** (bottom: different stoichiometric ratios of oxidant) measured in dichloromethane.

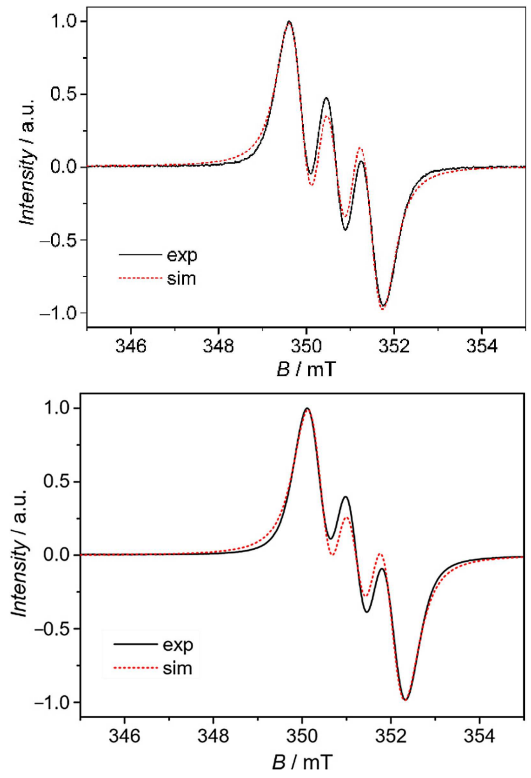

Figure 11. X-band ESR spectra for the oxidized ligand **4** (top) and complex **8** (bottom) measured in dichloromethane solution at room temperature ($c = 0.223$ mM for **4** and **8**; $c \approx 1$ mM for the oxidant).

species of the ligand **4** and complex **8** are depicted in Figure 11 (for ESR spectra of **2**, **3**, **6**, and **7** see Figure S25).

The observed *g* factor for all compounds is close to the expected value for the free electron at about 2.003 as expected for triarylamine radicals. The ESR spectra for the oxidized radical species of the methoxy substituted ligand **4** and complex **8** show a well-resolved hyperfine coupling of the electron spin to the nuclear spin of the nitrogen atom (^{14}N: $I = 1$) of the triphenylamine moiety of 22 MHz (0.79 mT). This is well within the expected range usually reported for triarylamine radicals.[4–5,39] A similar behavior is observed for the compounds with *tert*-butyl substitution (**3** and **7**) for which the hyperfine coupling is found to be 25 MHz (0.89 mT). For the methyl derivatives the hyperfine coupling is not resolved in the spectra (cf. Figure S25). Therefore, the hyperfine coupling can only be estimated to about 22 MHz (0.79 mT). The observed values for the hyperfine coupling constants are consistent with a nearly planar geometry at the nitrogen atom of the triphenylamine moiety as observed in the crystal structures.[38] Moreover, all radicals exhibit an isotropic signal with *g* values typical for triarylamine radicals. Comparing the ESR spectra and the fit parameters obtained from simulation it is obvious that there is very little variation between the ligands and their corresponding complexes, indicative for an only minor influence of the central dicopper unit on the coordinated triphenylamine radicals.

To further elucidate the character of possible interactions between the oxidized ligand backbone and the central paddle-wheel core, BS-DFT calculations for the corresponding radical cations of the complexes $[Cu_2(aba\text{-}R)_4(dmf)_2]^{4+}$ with fully oxidized triphenylamine moieties have been performed based on the molecular structures of the neutral complexes **5**–**8** derived from crystallography. The results of these BS-DFT calculations are summarized in Table S9 and the corresponding spin density distributions of the cationic radical species $\mathbf{5}^{4+}$–$\mathbf{8}^{4+}$ are depicted in Figures S26–S29. The data confirms that the unpaired spin density of the radicals is mainly localized at the central nitrogen atoms of the triphenylamine ligand moieties, which is in agreement with the observed hyperfine coupling in the ESR experiments. The BS-DFT calculations reveal a rather small ferromagnetic exchange coupling between the organic radicals and the copper(II) ions of the core unit in the order of 2–3 cm^{-1}. This again is consistent with the observed ESR spectra indicative of independent nitrogen-centered radicals. It should be noted that the exchange coupling between the two copper (II) ions within the paddle-wheel core is two orders of magnitude larger than their coupling with the coordinated radical cations, a situation which has also been observed for dinuclear copper paddle-wheel complexes with coordinated radical ligands on the basis of magnetic susceptibility measurements.[40] This consequently leads to a situation where the radical species can be regarded as virtually independent, which is consistent with the observations from ESR spectroscopy as well as electrochemistry.

Additional theoretical calculations to investigate the possible magnetic exchange between the organic radicals in the fully oxidized species have been performed utilizing the model systems $[Zn_2(aba\text{-}R)_4(dmf)_2]^{4+}$, where the copper ions have been replaced by zinc(II) ions. Generally, due to the arrangement of the four aryl carboxylates at the paddle-wheel core, two different magnetic couplings between the organic radicals are possible based on their relative position which can be *cis* or *trans* (J_{cis} and J_{trans}). The detailed results are summarized in Table S10 and the corresponding spin density distributions are depicted in Figures S30–S34. The BS-DFT calculations revealed an almost negligible antiferromagnetic coupling between the organic radicals for both possible type of interactions (J_{cis} = −0.09 to −0.22 cm^{-1}; J_{trans} = 0 to −0.09 cm^{-1}).

3. Conclusions

In summary, we have reported on four new monocarboxyl triphenylamine based ligands Haba-R (**1**–**4**) with varying substitution at the remaining *para* postilions of the phenyl rings and the corresponding dinuclear copper(II) complexes (**5**–**8**). All complexes adopt the common paddle-wheel arrangement for the dinuclear core, where the remaining axial coordination site at the copper(II) ions is occupied by a dmf molecule. The four complexes **5**–**8** have been fully characterized toward their structural and magnetic properties. A strong antiferromagnetic coupling between the copper(II) ions of the paddle-wheel core was observed and could be confirmed by BS-DFT calculations. Moreover, the variation of the substitution at the triphenylamine moieties did not show a significant influence on the observed magnetic exchange. Although triphenylamine derivatives have been widely studied due to their electrical conductivity, electroluminescence, and hole-transport properties, reports on their redox behavior and the interactions of their corresponding radical species within metal bonded systems are scarce. In the present work detailed electrochemical and spectroelectrochemical investigations of the triphenylamine-based ligands and complexes have been performed. For the *para* substituted ligands (**2**–**4**) and complexes (**6**–**8**) electrochemistry demonstrates the expected behavior leading to highly stable oxidized species for both ligands and complexes. Spectroelectrochemical experiments allowed us to characterize the properties of these oxidized radical species and to elucidate their interactions with the central dicopper core. It was found that the UV/vis and ESR spectroscopic properties do not significantly vary between the oxidized radical species derived from the ligands and the complexes, indicating that only small interactions between the radical species and the copper(II) ions can be present. This was further confirmed by BS-DFT calculations which show that the exchange interactions of the coordinated radicals with the copper(II) ions of the core unit are weak ferromagnetically coupled, but about two orders of magnitude smaller than the magnetic coupling within the dinuclear paddle-wheel core. Moreover, BS-DFT calculations for the fully oxidized complexes further indicate a very weak antiferromagnetic coupling among the ligand radicals. In the case of the presented complexes this leads to the observation of virtually independent radical species in the fully oxidized complex species $[Cu_2(aba\text{-}R)_4(dmf)_2]^{4+}$. This is most likely due to the fact that the dinuclear paddle-wheel core represents a strongly antiferromagnetically coupled unit with a diamagnetic singlet ground state. Nevertheless, triphenylamine derivatives as linkers can be regarded as promising candidates for obtaining new coordination polymers and MOFs that can lead to new magnetic materials via oxidation of the amine nitrogen leading to the generation of extra spin centers within the frameworks, which in turn can allow to transmit and trigger the magnetic exchange interactions between the paramagnetic metal ions of corresponding frameworks. However, this will preferentially require frameworks that contain metal ion building units, which are either based on mononuclear paramagnetic metal ions or exhibit magnetic interactions within the metal clusters that are in the same order of magnitude as those with the bridging linkers.

Experimental Section

Materials

All starting chemicals are commercially available and were used without further purification. The methyl 4-aminobenzoate was prepared as reported in literature.[41] Also the Buchwald–Hartwig coupling procedure utilized in the syntheses of the ligands **2**, **3**, and **4** was adapted from literature.[23] The syntheses of the complexes **5**, **6**, and **8** were carried out in Teflon-lined acid digestion vessels from Parr Instruments.

Physical Measurements

^1H and ^{13}C NMR spectra were recorded with Bruker Avance 400 and 600 MHz spectrometers. ^1H NMR assignments and comparison of the data for **1**–**4** are presented in Figure S35 and Table S11. Thermogravimetric analysis (TGA) on powdered samples was performed using a Netzsch STA409PC Luxx apparatus under constant flow of air ranging from room temperature up to 1000 °C with a heating rate of 5 °C min^{-1}. Mass spectra were measured on a Bruker MAT SSQ 710 spectrometer. Elemental analyses were determined on a Leco CHNS/932 and a VARIO EL III elemental analyzer. The FT-IR spectra were measured using the Specac Diamond ATR optional accessory on a VERTEX70 spectrometer by Bruker Optics. The UV/vis spectra were obtained on a Varian Cary5000 UV/vis/NIR spectrometer.

Syntheses

4-(Diphenylamino)benzaldehyde:[21] Triphenylamine (3.0 g, 12.2 mmol) was dissolved in dmf (150 mL) under stirring at 0 °C. The stirring was continued for 10 min and subsequently $POCl_3$ (1.2 mL) was added dropwise. After complete addition, the mixture was refluxed under N_2 atmosphere for 22 h. The dark mixture was then allowed to cool to room temperature and added into ice water (100 mL). The mixture was then neutralized with aqueous NaOH and extracted with CH_2Cl_2 (3×100 mL). The combined organic layers were washed with water (2×100 mL) and dried with anhydrous sodium sulphate. The product was then purified using flash column chromatography (hexane/ethyl acetate 5:1). Yield: 2.4 g, 72%; ^1H NMR (400 MHz, $CDCl_3$, 25 °C): δ = 9.81 (s, 1H, CHO),

7.68 (d, J=8.7 Hz, 2H), 7.34 (t, J=7.8 Hz, 2H), 7.15–7.19 (m, 6H), 7.02 ppm (d, J=8.7 Hz, 2H): ^{13}C NMR (100 MHz, $CDCl_3$, 25 °C): δ= 190.6, 153.5, 146.3, 131.5, 129.9, 129.3 126.5, 125.3, 119.5 ppm; IR (ATR, cm^{-1}): $\tilde{\upsilon}$=3063 (w), 1675 (s), 1581 (s), 1564 (m), 1487 (s), 1328 (s), 1285 (vs), 1218 (s), 1155 (m).

4-(Diphenylamino)benzoic acid (Haba, 1): To a solution of 4-(diphenylamino)benzaldehyde (2.0 g, 7.3 mmol) in acetone (60 mL) was added dropwise an aqueous solution (80 mL) containing K_2CO_3 (0.7 g, 5.1 mmol) and $KMnO_4$ (4.56 g, 29.2 mmol). The mixture was refluxed for 12 h overnight and subsequently filtered over a celite pad while still hot. The filtrate was then acidified using concentrated aqueous HCl, upon which the solution turned cloudy. The light yellow precipitate obtained was then filtered off, washed and dried overnight in an oven at 80 °C. Yield: 1.56 g, 76%; ^{1}H NMR (600 MHz, dmso-d_6, 25 °C): δ=12.48 (s, 1H, COOH), 7.79 (d, J= 8.8 Hz, 2H), 7.39 (t, J=7.9 Hz, 4H), 7.18 (t, J=7.4 Hz, 2H), 7.13 (d, J= 7.6 Hz, 4H), 6.88 ppm (d, J=8.8 Hz, 2H); ^{13}C NMR (151 MHz, dmso-d_6, 25 °C): δ=166.9, 151.3, 146.1, 130.8, 129.9, 125.7, 124.7, 122.4, 119.1 ppm; IR (ATR, cm^{-1}): $\tilde{\upsilon}$=3063 (w), 1665 (s), 1608 (m), 1583 (s), 1510 (m), 1488 (s), 1430 (m), 1415 (m), 1316 (s), 1271 (vs), 1177 (s), 1074 (m), 1028 (w), 949 (m); UV/vis spectra see Figure S36; EI-MS: m/z (%): 289 (100) $[M]^+$; elemental analysis calcd (%) for $C_{19}H_{15}NO_2$ (289.33 g mol^{-1}): C 78.87 H 5.23, N 4.84; found: C 78.64, H 5.11, N 4.89.

4-(Bis(4-tolylphenyl)amino)benzoic acid (Haba-Me, 2): To a solution of $Pd(OAc)_2$ (36 mg, 0.16 mmol) in degassed toluene (20 mL) P(t-Bu)$_3$ (0.19 mL, 0.48 mmol, 0.5 g mL^{-1} in hexane) was added, which was then stirred for 15 min at room temperature. Subsequently 4-bromotoluene (1.57 g, 9.6 mmol), methyl 4-aminobenzoate (0.48 g, 3.2 mmol), and Cs_2CO_3 (2.6 g, 8.0 mmol) were added to this solution. The resulting mixture was refluxed for 5 days. After this period the reaction mixture was allowed to cool to room temperature and poured into dichloromethane (60 mL). After filtration over a celite pad the filtrate was loaded onto silica gel by adding the silica (about 10 g) to the filtrate and evaporating all volatiles from the mixture. The loaded silica gel was used for flash column chromatography (chloroform/hexane 2:1) from which a yellow oil was obtained. A mixture of aqueous KOH solution (30 mL, 30%) and methanol (30 mL) was added and the reaction mixture refluxed overnight. Subsequently, the resulting mixture was filtered over a celite pad while still hot. The filtrate was acidified with concentrated aqueous HCl to give a colorless precipitate, which was filtered off, washed, and dried overnight in an oven at 80 °C. Yield: 0.65 g, 64%; ^{1}H NMR (400 MHz, dmso-d_6, 25 °C): δ=7.73 (d, J=8.9 Hz, 2H), 7.18 (d, J=8.2 Hz, 4H), 7.02 (t, J= 8.3 Hz, 4H), 6.77 (d, J=8.3 Hz, 2H), 2.28 ppm (s, 6H, Me); ^{13}C NMR (100 MHz, dmso-d_6, 25 °C): δ=167.04, 151.67, 143.53, 134.21, 130.42, 126.04, 121.44, 117.75, 20.51 ppm; IR (ATR, cm^{-1}): $\tilde{\upsilon}$ =3024 (w), 1667 (s), 1594 (s), 1505 (s), 1416 (m), 1315 (s), 1280 (vs), 1175 (s), 949 (w); UV/vis spectra see Figure S37; EI-MS: m/z (%): 317 (100) $[M]^+$; elemental analysis calcd (%) for $C_{21}H_{19}NO_2$ (317.38 g mol^{-1}): C 79.47, H 6.03, N 4.41; found: C 79.53, H 5.99, N 4.43.

4-(Bis(4-*tert*-butylphenyl)amino)benzoic acid (Haba-tBu, 3): The procedure described for **2** was adopted for the coupling of 4-*tert*-butylbromobenzene (1.7 mL, 9.9 mmol) utilizing the similar reaction conditions and compounds ($Pd(OAc)_2$: 37 mg, 0.17 mmol; P(t-Bu)$_3$: 0.20 mL, 0.5 mmol; methyl-4-aminobenzoate: 0.50 g, 3.3 mmol; Cs_2CO_3: 2.7 g, 8.3 mmol) as well as solvent (toluene: 20 mL). The final reaction mixture was allowed to cool to room temperature and poured into dichloromethane (60 mL). After filtration over a celite pad the filtrate was loaded onto silica gel by adding the silica (about 10 g) to the filtrate and evaporating all volatiles from the mixture. The loaded silica gel was used for flash column chromatography (chloroform/hexane 2:1) from which a brown solid was obtained. A mixture of aqueous KOH solution (30 mL, 30%) and methanol (60 mL) was added and the mixture refluxed overnight. The reaction mixture was then filtered hot over a celite pad and subsequently acidified with concentrated aqueous HCl to give a colorless precipitate, which was filtered off, washed, and dried overnight in an oven at 80 °C. Yield: 0.97 g, 91%; ^{1}H NMR (400 MHz, dmso-d_6, 25 °C) δ=7.74 (d, J=8.9 Hz, 2H), 7.38 (d, J= 8.2 Hz, 4H), 7.05 (d, J=8.3 Hz, 4H), 6.78 (d, J=8.3 Hz, 2H), 1.27 ppm (s, 18H, CMe_3); ^{13}C NMR (100 MHz, dmso-d_6, 25 °C) δ=167.5, 152.0, 147.7, 143.8, 131.3, 127.1, 125.1, 122.0, 118.3, 34.7, 31.6 ppm; IR (ATR, cm^{-1}): $\tilde{\upsilon}$=3024 (w), 1667 (s), 1594 (s), 1505 (s), 1416 (m), 1315 (s), 1280 (vs), 1175 (s), 949 (w); UV/vis spectra see Figure S38; EI-MS: m/z (%): 401 (85) $[M]^+$; elemental analysis calcd (%) for $C_{27}H_{31}NO_2$ (401.54 g mol^{-1}): C 80.76, H 7.78, N 3.49; found: C 80.96, H 7.89, N 3.50.

4-(Bis(4-methoxyphenyl)amino)benzoic acid (Haba-OMe, 4): The procedure described for **2** was adopted for the coupling of 4-bromoanisole (3 mL, 23.7 mmol) utilizing the similar reaction conditions and compounds ($Pd(OAc)_2$: 88 mg, 0.4 mmol; P(t-Bu)$_3$: 0.48 mL, 1.2 mmol; methyl 4-aminobenzoate: 1.2 g, 7.9 mmol; Cs_2CO_3: 6.6 g, 19.8 mmol) as well as solvent (toluene: 20 mL). The reaction mixture was allowed to cool to room temperature and poured into dichloromethane (150 mL). After filtration over a celite pad the filtrate was loaded onto silica gel by adding the silica (about 10 g) to the filtrate and evaporating all volatiles from the mixture. The loaded silica gel was used for flash column chromatography (chloroform/hexane 2:1) from which a colorless oil was obtained. A mixture of aqueous KOH solution (30 mL, 30%) and methanol (30 mL) was added and the mixture refluxed overnight. The resulting mixture was filtered hot over a celite pad followed by acidification with concentrated aqueous HCl to give a light brown precipitate, which was filtered off, washed, and dried overnight in an oven at 80 °C. Yield: 1.22 g, 46%; ^{1}H NMR (400 MHz, $CDCl_3$, 25 °C) δ=7.84 (d, J=8.9 Hz, 2H), 7.12 (t, J=8.9 Hz, 4H), 6.88 (d, J=8.9 Hz, 4H), 6.81 (d, J=8.9 Hz, 2H), 3.81 ppm (s, 6H, OMe); ^{13}C NMR (100 MHz, $CDCl_3$, 25 °C) δ=171.1, 157.0, 153.4, 139.3, 131.6, 127.9, 119.0, 116.8, 115.0, 55.3 ppm; IR (ATR, cm^{-1}): $\tilde{\upsilon}$=3394 (w), 1666 (s), 1594 (m), 1502 (m), 1462 (m), 1317 (s), 1280 (vs), 1174 (s), 1126 (w), 1033 (w), 930 (w); UV/vis spectra see Figure S39; EI-MS: m/z (%): 349 (100) $[M]^+$; elemental analysis calcd (%) for $C_{21}H_{19}NO_4$ (349.38 g mol^{-1}): C 72.19, H 5.48, N 4.01; found: C 72.02, H 5.38, N 4.09.

$[Cu_2(aba)_4(dmf)_2]$ (5): A mixture of the ligand Haba (**1**, 0.05 g, 0.173 mmol) and $Cu(NO_3)_2 \cdot 3H_2O$ (0.08 g, 0.34 mmol) in dmf (4 mL) was stirred for 1 h. The resulting green solution was transferred into a 23 mL Teflon-walled Parr acid digestion bomb. The reaction container was placed in an oven and heated at 110 °C for 24 h under autogenous pressure followed by cooling at a constant rate of 0.2 °C min^{-1}. Allowing the resulting reaction solution to stand for a few hours at room temperature led to the formation of green crystals from the brown mother liquor. The crystals were filtered off, washed with dmf until the wash fluid was no longer colored and dried in vacuo. Yield: 48 mg, 66%; IR (ATR, cm^{-1}): $\tilde{\upsilon}$=1667 (m), 1608 (s), 1587(s), 1558 (w), 1488 (m), 1391 (vs), 1317 (m), 1274 (s), 1176 (m), 1100 (w), 1090 (w); UV/vis spectra see Figure S36; elemental analysis calcd (%) for **5**·4 dmf, $C_{94}H_{98}Cu_2N_{10}O_{14}$ (1718.93 g mol^{-1}): C 65.68, H 5.75, N 8.15; found: C 66.10, H 5.74, N 8.05.

$[Cu_2(aba\text{-}Me)_4(dmf)_2]$ (6): The ligand Haba-Me (**2**, 0.15 g, 0.476 mmol) and $Cu(NO_3)_2 \cdot 3H_2O$ (0.23 g, 0.952 mmol) were dissolved in dmf (4 mL) and stirred overnight. The resulting green solution was then transferred into a 23 mL Teflon-walled Parr acid digestion bomb. The reaction vessel was placed in an oven to heat at 110 °C for 24 h under autogenous pressure followed by cooling at a constant rate of 0.2 °C min^{-1}. The insoluble products were separated by centrifugation leading to a clear supernatant, which

was separated and carefully layered by methanol (1 mL) on top. However, the solvent layer separation disappeared within about 15 min leading to a clear solution from which a light green precipitate was formed after a few hours. The precipitate was filtered off and washed with methanol. Additional product could be isolated from the filtrate as green block crystals after allowing it to stand for a few days. The combined product was dried in vacuo. Yield: 126 mg, 68%; IR (ATR, cm^{-1}): $\tilde{\nu}$ = 1667 (m), 1608 (s), 1599 (s), 1504 (s), 1394 (vs), 1316 (s), 1267 (s), 1169 (s); UV/vis spectra see Figure S37; elemental analysis calcd (%) for **6**·1.5H_2O, $C_{90}H_{89}Cu_2N_6O_{11.5}$ (1565.79 g mol^{-1}) C 69.04, H 5.73, N 5.37 found: C 68.73, H 5.46, N 5.43.

[Cu_2(aba-tBu)$_4$(dmf)$_2$] (7): A mixture of the ligand Haba-tBu (**3**, 0.05 g, 0.124 mmol) and $Cu(NO_3)_2 \cdot 3H_2O$ (0.03 g, 0.124 mmol) in dmf (2 mL) was stirred for 1 h followed by heating at 110 °C for 30 min. The resulting green solution was allowed to stand leading to green crystals being formed after a few days. The crystalline material was separated, washed with dmf, and dried in vacuo for 4 h to obtain the dried material. Yield: 39 mg, 16%; IR (ATR, cm^{-1}): $\tilde{\nu}$ = 2962 (m), 1671 (s), 1699 (s), 1506 (s), 1485 (s) 1397 (vs), 1321 (s), 1267 (m), 1176 (s), 1146 (w), 1063 (m); UV/vis spectra see Figure S38; elemental analysis calcd (%) for **7**·dmf·H_2O, $C_{117}H_{143}Cu_2N_7O_{12}$ (1966.51 g mol^{-1}): C 71.46, H 7.33, N 4.99; found: C 71.52, H 7.11, N 4.95.

[Cu_2(aba-OMe)$_4$(dmf)$_2$] (8): Solutions of the ligand Haba-OMe (4, 0.04 g, 0.114 mmol) in dmf (1.5 mL) and $Cu(NO_3)_2 \cdot 3H_2O$ (0.014 g, 0.057 mmol) in dmf (1.5 mL) were mixed in a 23 mL Teflon-walled Parr acid digestion bomb and stirred for 1 h at room temperature. Subsequently, the mixture was heated under autogenous pressure at 110 °C for 24 h followed by cooling at a constant rate of 0.2 °C min^{-1}. From the mother liquor which was allowed to stand undisturbed dark green micro-crystals were obtained. The micro-crystalline material was filtered off, washed with dmf until the wash fluid was no longer colored, and dried for 1 h in vacuo. Crystals suitable for X-ray studies were obtained by stirring a mixture of ligand and metal salt in dmf for about 20 min followed by slowly layering methanol on top of the mixture. Both solvents were allowed to slowly evaporate over 4 weeks to yield green crystals of **8**, which were dried in vacuo. Yield: 61 mg, 32%; IR (ATR, cm^{-1}): $\tilde{\nu}$ = 1660 (m), 1600 (s), 1557 (s), 1391 (vs), 1319 (s), 1274 (m), 1239 (vs), 1182 (s), 1144 (w), 1088 (m); UV/vis spectra see Figure S39; elemental analysis calcd (%) for $C_{90}H_{86}Cu_2N_6O_{18}$ (1666.77 g mol^{-1}): C 64.85, H 5.20, N 5.04; found: C 64.95, H 5.16, N 5.37.

Synthesis of Radical Cations

Excess of silver tetrafluoroborate (2 mM in CH_2Cl_2) was added into dilute solutions of the compounds in dichloromethane ($\approx 10^{-4}$ M) leading to deep blue-violet solutions which were centrifuged. The clear supernatant was decanted off and used for collection of ESR as well as UV/vis spectroscopic data. The obtained solutions of the oxidized radical cations were observed to be stable for several days, as no spectral changes could be detected within this period.

Voltammetry

CV measurements: Cyclic voltammetry measurements were carried out at room temperature using a Reference 600 potentiostat (GAMRY Instruments). For the measurements of the ligand Haba (**1**) and its copper complex **5** in dichloromethane solution a Pt electrode was employed with 0.1 M tetrabutylammonium perchlorate (TBAP) as co-electrolyte. A scan rate of 1 Vs^{-1} was used and the reference electrode was a Ag/AgCl electrode.

Square-wave measurements: Square-wave voltammetric measurements were conducted on the substituted ligand analogues **2**–**4** and their copper complexes **6**–**8**, utilizing a three-electrode technique using the same potentiostat as above. The instrument was controlled by the DigiElch 8 software (available from GAMRY). This program provides not only routines for the digital simulation of electrochemical experiments but also those for performing the measurements in a consistent way making use of the GAMRY Electrochemical Toolkit library. The square-wave voltammograms were measured in dichloromethane (containing 0.25 M tetra-*n*-hexylammoniumperchlorate) under a blanket of solvent-saturated nitrogen gas using a square-wave signal with an amplitude of 25 mV and potential steps of 5 mV in all experiments. The ohmic resistance, which had to be compensated for, was determined by measuring the impedance of the system at potentials where the faradaic current was negligibly small. Background correction was accomplished by subtracting the current curves of the blank electrolyte (containing the same concentration of supporting electrolyte) from the experimental square-wave voltammograms. The working electrode was an 1.6 mm carbon disk electrode (ALS Japan). A Ag/AgCl electrode in acetonitrile containing 0.25 M tetra-*n*-butylammonium chloride served as reference electrode. All potentials reported in this paper refer to the ferrocenium/ferrocene couple, which was always measured at the end of a series of experiments.

Spectroelectrochemistry

Spectroelectrochemical experiments were performed using the Reference 600 potentiostat in combination with an AvaSpec 2048 spectrometer and an AvaLight-DHc light-source (both from Avantes, Apeldoorn, The Netherlands). The synchronization between potentiostat and spectrometer as well as the simultaneous recording of spectra and current curve was accomplished by the SPELCH software module included in DigiElch 8. A commercially available optically transparent thin-layer electrochemical (OTTLE) cell (University of Reading) with an optical path length of about 0.2 mm was used in all experiments. The cell consists of two platinum net electrodes serving as working and counter electrode. The (pseudo-)reference electrode is a silver wire. All spectra are difference spectra with respect to the spectrum of the starting material, which was taken as reference spectrum.

Magnetic Measurements and ESR Spectroscopy

The magnetic susceptibility was measured on bulk vacuum dried materials in the 4–300 K temperature range with a Quantum Design MPMS-5 superconducting SQUID magnetometer. The measured data were corrected for diamagnetism of the capsules used and the intrinsic diamagnetism of the constituent atoms using Pascal constants. The ESR spectra were recorded at room temperature using an X-Band ELEXSYS E500 spectrometer from Bruker equipped with a SHQE resonator. The simulation of the experimental data was performed with EasySpin.[42]

X-ray Diffraction

The single crystal X-ray data for the compounds **5**–**8** were collected on a Nonius KappaCCD diffractometer, using graphite-monochromated Mo–K radiation (λ = 71.073 pm). Data were corrected for Lorentz and polarization effects, absorption was taken into account on a semi-empirical basis using multiple scans.[43] The structures were solved by direct methods (SHELXS[44]) and refined by full-matrix least squares techniques against F_o^2 (SHELXL-2014[44]). All hydrogen atoms were included at calculated positions with fixed

thermal parameters. All non-disordered, non-hydrogen atoms were refined anisotropically.[44] The crystals of **5** and **7** contain large voids, filled with disordered solvent molecules, with a size of 821 and 554×10^6 pm^3/unit cell for **5** and **7**, respectively. Their contribution to the structure factors of **5** and **7** were secured by back-Fourier transformation using the SQUEEZE routine of the program PLATON[45] resulting in 225 and 151 electrons/unit cell, respectively. Crystallographic data as well as structure solution and refinement details are summarized in Table S2. Diamond 4.2.2,[46] Olex 1.2.9,[47] and ORTEP-3[48] were used for structure representations. CCDC 1521017–1521020 contain the supplementary crystallographic data for complexes **5**–**8**. These data are provided free of charge by the Cambridge Crystallographic Data Centre (http://www.ccdc.cam.ac.uk). The powder measurements were performed on a Stoe Powder Diffractometer with a Mythen 1 K detector at room temperature. Measurements were done using capillary tubes while the Debye–Scherrer Scan Mode was applied with a 2θ scan type. The X-ray tube was a Cu-long fine focus tube. The measurement was carried out between 2 and 50° with steps of 2.1° per 20 seconds.

Computational Details

The structures used for calculations are based on the single-crystal structure data of **5**–**8** as all atomic positions of non-hydrogen atoms are concerned. The positions of all hydrogen atoms were optimized in the high-spin state ($S=1$) at RI-DFT[49]/PBE[50]/def2-SVP[51] level of theory utilizing the TURBOMOLE 6.6 package of programs.[52] For broken-symmetry DFT (BS-DFT) calculations the PBE0 hybrid functional[50,53] was employed in combination with highly polarized triple-ζ def2-TZVPP basis sets.[51] The coupling constants were obtained by Yamaguchi's approach (Equation (7)) for an isotropic Heisenberg Hamiltonian ($\hat{H} = -J\hat{S}_1\hat{S}_2$.).[54]

$$J = \frac{2(E_{BS} - E_{HS})}{\langle S^2_{HS}\rangle - \langle S^2_{BS}\rangle} \quad (7)$$

Acknowledgements

O.A. thanks the Evangelisches Studienwerk Villigst and the Graduierten Akademie of the Friedrich-Schiller-Universität Jena for scholarships. We also thank Mr. Reinhardt for the measurement of the thermogravimetric and magnetic data and Mrs. Wermann for measuring the powder diffraction data. Finally, we want to thank the URZ Jena for providing additional computational resources.

Conflict of Interest

The authors declare no conflict of interest.

Keywords: copper · molecular electrochemistry · magnetic properties · carboxylate ligands · density functional calculations

[1] a) R. Rybakiewicz, M. Zagorska, A. Pron, *Chem. Pap.* **2017**, *71*, 243–268; b) A. Mahmood, *Chem. Soc. Rev.* **2016**, *123*, 127–144; c) M. Liang, J. Chen, *Chem. Soc. Rev.* **2013**, *42*, 3453–3488; d) Y. Shirota, H. Kageyama, *Chem. Rev.* **2007**, *107*, 953–1010.

[2] a) R. A. Klenkler, G. Voloshin, *J. Phys. Chem. C* **2011**, *115*, 16777–16781; b) P. Cias, C. Slugovc, G. Gescheidt, *J. Phys. Chem. A* **2011**, *115*, 14519–14525; c) P. M. Borsenberger, E. H. Magin, *Macromol. Symp.* **1997**, *116*, 51–58; d) C. W. Tang, S. A. VanSlyke, *Appl. Phys. Lett.* **1987**, *51*, 913–915.

[3] a) U. Mitschke, P. Bäuerle, *J. Mater. Chem.* **2000**, *10*, 1471–1507; b) G. Wu, G. Zhao, C. He, J. Zhang, Q. He, X. Chen, Y. Li, *Sol. Energy Mater. Sol. Cells* **2009**, *93*, 108–113; c) O. Alévêque, P. Leriche, N. Cocherel, P. Frére, A. Cravino, J. Roncali, *Sol. Energy Mater. Sol. Cells* **2008**, *92*, 1170–1174; d) C. He, Q. He, X. Yang, G. Wu, C. Yang, F. Bai, Z. Shuai, L. Wang, Y. Li, *J. Phys. Chem. C* **2007**, *111*, 8661–8666; e) S. Roquet, A. Cravino, P. Leriche, O. Alévêque, P. Frére, J. Roncali, *J. Am. Chem. Soc.* **2006**, *128*, 3459–3466.

[4] R. I. Walter, *J. Am. Chem. Soc.* **1966**, *88*, 1923–1930.

[5] E. T. Seo, R. F. Nelson, J. M. Fritsch, L. S. Marcoux, D. W. Leedy, R. N. Adams, *J. Am. Chem. Soc.* **1966**, *88*, 3498–3503.

[6] J.-H. Pan, H.-L. Chiu, L. Chen, B.-C. Wang, *Comput. Mater. Sci.* **2006**, *38*, 105–112.

[7] B. Adelizzi, I. A. W. Filot, A. R. A. Palmans, E. W. Meijer, *Chem. Eur. J.* **2017**, *23*, 6103–6110.

[8] a) H. Iden, W. Bi, J.-F. Morin, F.-G. Fontaine, *Inorg. Chem.* **2014**, *53*, 2883–2891; b) M. Zhu, Y. Li, C. t. Li, C. Zhong, C. Yang, H. Wu, J. Qin, Y. Cao, *J. Mater. Chem.* **2012**, *22*, 11128–11133; c) Y. Liu, Y. Wang, H. Guo, M. Zhu, C. Li, J. Peng, W. Zhu, Y. Cao, *J. Phys. Chem. C* **2011**, *115*, 4209–4216; d) J. Wang, C. He, P. Wu, J. Wang, C. Duan, *J. Am. Chem. Soc.* **2011**, *133*, 12402–12405; e) L. Zhang, B. Li, S. Yue, M. Li, Z. Hong, W. Li, *J. Lumin.* **2008**, *128*, 620–624; f) G. S. Maciel, K.-S. Kim, S.-J. Chung, J. Swiatkiewicz, G. S. He, P. N. Prasad, *J. Phys. Chem. B* **2001**, *105*, 3155–3157.

[9] a) L. Chen, S. Mallick, Y. N. Tan, M. Meng, C. Y. Liu, *Inorg. Chem.* **2017**, *56*, 7470–7481; b) M. H. Chisholm, C. B. Durr, S. A. Lewis, *Polyhedron* **2013**, *64*, 339–345.

[10] S. I. Vagin, A. K. Ott, B. Rieger, *Chem. Ing. Tech.* **2007**, *79*, 767–780.

[11] a) J. N. V. Niekerk, F. R. L. Schoening, *Acta Crystallogr.* **1953**, *6*, 227–232; b) B. Bleaney, K. D. Bowers, *Proc. R. Soc. Edinburgh Sect. A* **1952**, *214*, 451–465; c) B. C. Guha, *Proc. R. Soc. Edinburgh Sect. A* **1951**, *206*, 353–373; d) M. Melnik, *Coord. Chem. Rev.* **1982**, *42*, 259–293.

[12] S. S. Chui, S. M.-F. Lo, J. P. H. Charmant, A. G. Orpen, I. D. William, *Science* **1999**, *283*, 1148–1150.

[13] a) X. X. Zhang, S. S.-Y. Chui, I. D. Williams, *J. Appl. Phys.* **2000**, *87*, 6007–6009; b) W. Böhlmann, A. Pöppl, M. Sabo, S. Kaskel, *J. Phys. Chem. B* **2006**, *110*, 20177–20181; c) S. Ketrat, T. Maihom, S. Wannakao, M. Probst, S. Nokbin, J. Limtrakul, *Inorg. Chem.* **2017**, *56*, 14005–14012; d) M. K. Bhunia, J. T. Hughes, J. C. Fettinger, A. Navrotsky, *Langmuir* **2013**, *29*, 8140–8145; e) X.-S. Wang, S. Ma, P. M. Forster, D. Yuan, J. Eckert, J. J. López, B. J. Murphy, J. B. Parise, H.-C. Zhou, *Angew. Chem.* **2008**, *120*, 7373–7376; *Angew. Chem. Int. Ed.* **2008**, *47*, 7263–7266; f) B. Chen, N. W. Ockwig, A. R. Millward, D. S. Contreras, O. M. Yaghi, *Angew. Chem.* **2005**, *117*, 4823–4827; *Angew. Chem. Int. Ed.* **2005**, *44*, 4745–4749; g) M. Eddaoudi, J. Kim, J. B. Wachter, H. K. Chae, M. O'Keeffe, O. M. Yaghi, *J. Am. Chem. Soc.* **2001**, *123*, 4368–4369; h) K. Tan, N. Nijem, P. Canepa, Q. Gong, J. Li, T. Thonhauser, Y. J. Chabal, *Chem. Mater.* **2012**, *24*, 3153–3167; i) S. Rostamnia, H. Alamgholiloo, M. Jafari, R. Rookhosh, A. R. Abbasib, *Appl. Organomet. Chem.* **2016**, *30*, 954–958; j) S. Krause, V. Bon, I. Senkovska, U. Stoeck, D. Wallacher, D. M. Többens, S. Zander, R. S. Pillai, G. Maurin, F.-X. Coudert, S. Kaskel, *Nature* **2016**, *532*, 348–352.

[14] a) H. K. Chae, J. Kim, O. D. Friedrichs, M. O'Keeffe, O. M. Yaghi, *Angew. Chem.* **2003**, *115*, 4037–4039; *Angew. Chem. Int. Ed.* **2003**, *42*, 3907–3909; b) E. Y. Lee, S. Y. Jang, M. P. Suh, *J. Am. Chem. Soc.* **2005**, *127*, 6376–6381; c) O. Akintola, D. Hornig, A. Buchholz, H. Görls, W. Plass, *Dalton Trans.* **2017**, *46*, 8037–8050; d) C. Livage, N. Guillou, A. Castiglione, J. Marrot, M. Frigoli, F. Millange, *Microporous Mesoporous Mater.* **2012**, *157*, 37–41; e) Y. Shen, X.-F. Yang, H.-B. Zhu, Y. Zhao, W.-S. Li, *Dalton Trans.* **2015**, *44*, 14741–14746; f) Q. Yao, A. B. Gómez, J. Su, V. Pascanu, Y. Yun, H. Zheng, H. Chen, L. Liu, H. N. Abdelhamid, B. Martín-Matute, X. Zou, *Chem. Mater.* **2015**, *27*, 5332–5339; g) J.-S. Hu, L. Zhang, L. Qin, H.-G. Zheng, X.-B. Zhang, *Chem. Commun.* **2015**, *51*, 2899–2902; h) X.-L. Hu, F.-H. Liu, C. Qin, K.-Z. Shao, Z.-M. Su, *Dalton Trans.* **2015**, *44*, 7822–7827; i) X.-L. Hu, C. Qin, X.-L. Wang, K.-Z. Shao, Z.-M. Su, *New J. Chem.* **2015**, *39*, 7858–7862; j) M. Venkateswarulu, A. Pramanik, R. R. Koner, *Dalton Trans.* **2015**, *44*, 6348–6352; k) Y. Li, Z. Weng, Y. Wang, L. Chen, D. Sheng, J. Diwu, Z. Chai, T. E. Albrecht-Schmitt, S. Wang, *Dalton Trans.* **2016**, *45*, 918–921; l) Y.-F. Niu, L.-T. Cui, J. Han, X.-L. Zhao, *J. Solid State Chem.* **2016**, *241*, 18–25; m) C. Qiao, X. Qu, Q. Yang, Q. Wei, G. Xie, S. Chen, D. Yang, *Green Chem.* **2016**, *18*, 951–956; n) Y.-J. Qu, J. Li, *Inorg. Chem. Commun.* **2017**, *76*, 77–80.

[15] a) P. Wu, J. Wang, C. He, X. Zhang, Y. Wang, T. Liu, C. Duan, *Adv. Funct. Mater.* **2012**, *22*, 1698–1703; b) Z. Peng, X. Yi, Z. Liu, J. Shang, D. Wang,

ACS Appl. Mater. Interfaces **2016**, *8*, 14578–14585; c) X.-L. Hu, C. Qin, X.-L. Wang, K.-Z. Shao, Z.-M. Su, *Chem. Commun.* **2015**, *51*, 17521–17524; d) M. Zhang, J. Han, H. Wu, Q. Wei, G. Xie, S. Chen, S. Gao, *RSC Adv.* **2016**, *6*, 94622–94628; e) D.-M. Chen, J.-Y. Tian, C.-S. Liu, *Inorg. Chem. Commun.* **2016**, *68*, 29–32; f) L. Wen, X. Wang, H. Shi, K. Lv, C. Wang, *RSC Adv.* **2016**, *6*, 1388–1394; g) Y. Du, N. Song, X. Lv, B. Hu, W. Zhou, Q. Jia, *Dyes Pigm.* **2017**, *138*, 15–22; h) P. Wu, J. Wang, Y. Li, C. He, Z. Xie, C. Duan, *Adv. Funct. Mater.* **2011**, *21*, 2788–2794; i) P. Wu, C. He, J. Wang, X. Peng, X. Li, Y. An, C. Duan, *J. Am. Chem. Soc.* **2012**, *134*, 14991–14999; j) P. Wu, X. Guo, L. Cheng, C. He, J. Wang, C. Duan, *Inorg. Chem.* **2016**, *55*, 8153–8159; k) Y. E. Cheon, M. P. Suh, *Angew. Chem.* **2009**, *121*, 2943–2947; *Angew. Chem. Int. Ed.* **2009**, *48*, 2899–2903.

[16] a) P. M. Usov, C. Fabian, D. M. D'Alessandro, *Chem. Commun.* **2012**, *48*, 3945–3947; b) F. J. Rizzuto, T. B. Faust, B. Chan, C. Hua, D. M. D'Alessandro, C. J. Kepert, *Chem. Eur. J.* **2014**, *20*, 17597–17605; c) C. Hua, A. Baldansuren, F. Tuna, D. Collison, D. M. D'Alessandro, *Inorg. Chem.* **2016**, *55*, 7270–7280.

[17] a) C. F. Leong, T. B. Faust, P. Turner, P. M. Usov, C. J. Kepert, R. Babarao, A. W. Thornton, D. M. D'Alessandro, *Dalton Trans.* **2013**, *42*, 9831–9839; b) C. F. Leong, B. Chan, T. B. Faust, D. M. D'Alessandro, *Chem. Sci.* **2014**, *5*, 4724–4728; c) C. Hua, B. F. Abrahams, D. M. D'Alessandro, *Cryst. Growth Des.* **2016**, *16*, 1149–1159.

[18] a) K. Koh, A. G. Wong-Foy, A. J. Matzger, *J. Am. Chem. Soc.* **2010**, *132*, 15005–15010; b) A. Dutta, A. G. Wong-Foy, A. J. Matzger, *Chem. Sci.* **2014**, *5*, 3729–3734; c) L.-T. Cui, Y.-F. Niu, J. Han, X.-L. Zhao, *J. Solid State Chem.* **2015**, *227*, 155–164; d) L. Yang, S. Zhang, X. Qu, Q. Yang, X. Liu, Q. Wei, G. Xie, S. Chen, *J. Solid State Chem.* **2015**, *231*, 223–229; e) S. J. Lee, C. Doussot, A. Baux, L. Liu, G. B. Jameson, C. Richardson, J. J. Pak, F. Trousselet, F.-X. Coudert, S. G. Telfer, *Chem. Mater.* **2016**, *28*, 368–375; f) O. Akintola, S. Ziegenbalg, A. Buchholz, H. Görls, W. Plass, *CrystEngComm* **2017**, *19*, 2723–2732; g) S. J. Lee, C. Doussot, S. G. Telfer, *Cryst. Growth Des.* **2017**, *17*, 3185–3191.

[19] a) D. Sun, D. J. Collins, Y. Ke, J.-L. Zuo, H.-C. Zhou, *Chem. Eur. J.* **2006**, *12*, 3768–3776; b) Y. E. Cheon, J. Park, M. P. Suh, *Chem. Commun.* **2009**, 5436–5438; c) H. J. Park, Y. E. Cheon, M. P. Suh, *Chem. Eur. J.* **2010**, *16*, 11662–11669; d) R. Grünker, I. Senkovska, R. Biedermann, N. Klein, A. Klausch, I. A. Baburin, U. Müller, S. Kaskel, *Eur. J. Inorg. Chem.* **2010**, 3835–3841; e) R. Grünker, I. Senkovska, R. Biedermann, N. Klein, M. R. Lohe, P. Müller, S. Kaskel, *Chem. Commun.* **2011**, *47*, 490–492; f) X. Li, X. Chen, F. Jiang, L. Chen, S. Lu, Q. Chen, M. Wu, D. Yuan, M. Hong, *Chem. Commun.* **2016**, *52*, 2277–2280; g) X. Li, F. Jiang, L. Chen, M. Wu, S. Lu, J. Pang, K. Zhou, X. Chen, M. Hong, *CrystEngComm* **2016**, *18*, 2239–2243; h) P. Müller, F. M. Wisser, V. Bon, R. Grünker, I. Senkovska, S. Kaskel, *Chem. Mater.* **2015**, *27*, 2460–2467; i) P. Müller, V. Bon, I. Senkovska, J. Getzschmann, M. S. Weiss, S. Kaskel, *Cryst. Growth Des.* **2017**, *17*, 3221–3228; j) P. Müller, F. M. Wisser, P. Freund, V. Bon, I. Senkovska, S. Kaskel, *Inorg. Chem.* **2017**, *56*, 14164–14169.

[20] H. K. Chae, M. Eddaoudi, J. Kim, S. I. Hauck, J. F. Hartwig, M. O'Keeffe, O. M. Yaghi, *J. Am. Chem. Soc.* **2001**, *123*, 11482–11483.

[21] G. Lai, X. Bu, J. Santos, *Synlett* **1997**, 1275–1276.

[22] B. Liu, Q. Zhang, H. Ding, G. Hu, Y. Du, C. Wang, J. Wu, S. Li, H. Zhou, J. Yang, Y. Tian, *Dyes Pigm.* **2012**, *95*, 149–160.

[23] R. Lartia, C. Allain, G. Bordeau, F. Schmidt, C. Fiorini-Debuisschert, F. Charra, M.-P. Teulade-Fichou, *J. Org. Chem.* **2008**, *73*, 1732–1744.

[24] a) K. Sreenath, T. G. Thomas, K. R. Gopidas, *Org. Lett.* **2011**, *13*, 1134–1137; b) S. Sumalekshmy, K. R. Gopidas, *Chem. Phys. Lett.* **2005**, *413*, 294–299.

[25] B. A. Blight, A. F. Stewart, N. Wang, S. W. J.-S. Lu, *Inorg. Chem.* **2012**, *51*, 778–780.

[26] O. Kahn, *Molecular Magnetism*, Wiley-VCH Inc., Weinheim, **1993**.

[27] a) J. P. Naskar, C. Biswas, B. Guhathakurta, N. Aliaga-Alcalde, L. Lu, M. Zhu, *Polyhedron* **2011**, *30*, 2310–2319; b) A. Aijaz, E. C. Sanudo, P. K. Bharadwaj, *Inorg. Chim. Acta* **2009**, *362*, 4246–4250.

[28] N. F. Chilton, R. P. Anderson, L. D. Turner, A. Soncini, K. S. Murray, *J. Comput. Chem.* **2013**, *34*, 1164–1175.

[29] a) D. Plaul, D. Geibig, H. Görls, W. Plass, *Polyhedron* **2009**, *28*, 1982–1990; b) E. T. Spielberg, M. Fittipaldi, D. Geibig, D. Gatteschi, W. Plass, *Inorg. Chim. Acta* **2010**, *363*, 4269–4276; c) E. T. Spielberg, A. Gilb, D. Plaul, D. Geibig, D. Hornig, D. Schuch, A. Buchholz, A. Ardavan, W. Plass, *Inorg. Chem.* **2015**, *54*, 3432–3438.

[30] C.-C. Chang, M.-k. Leung, *Chem. Mater.* **2008**, *20*, 5816–5821.

[31] a) M. Oyama, K. Nozaki, S. Okazaki, *Anal. Chem.* **1991**, *63*, 1387–1392; b) T. Zhang, A. Brajter-Toth, *Anal. Chem.* **2000**, *72*, 2533–2540; c) O. Yurchenko, D. Freytag, L. Z. Borg, R. Zentel, J. Heinze, S. Ludwigs, *J. Phys. Chem. B* **2012**, *116*, 30–39.

[32] a) C. Quinton, V. Alain-Rizzo, C. Dumas-Verdes, F. Miomandr, P. Audebert, *Electrochim. Acta* **2013**, *110*, 693–701; b) C.-J. Yao, Y.-W. Zhong, J. Yao, *Inorg. Chem.* **2013**, *52*, 10000–10008.

[33] J. M. Olmos, A. Molina, E. Laborda, F. Martínez-Ortiz, *Electrochim. Acta* **2015**, *176*, 1044–1053.

[34] S. Dapperheld, E. Steckhan, K.-H. G. Brinkhaus, T. Esch, *Chem. Ber.* **1991**, *124*, 2557–2567.

[35] a) B. Jin, P. Liu, Y. Wang, Z. Zhang, Y. Tian, J. Yang, S. Zhang, F. Cheng, *J. Phys. Chem. B* **2007**, *111*, 1517–1522; b) W. H. Morrison, S. Krogsrud, D. N. Hendrickson, *Inorg. Chem.* **1973**, *12*, 1998–2004.

[36] a) J. B. Flanagan, S. Margel, A. J. Bard, F. C. Anson, *J. Am. Chem. Soc.* **1978**, *100*, 4248–4253; b) F. Ammar, J. M. Savéant, *J. Electroanal. Chem. Interfacial Electrochem.* **1973**, *47*, 215–221.

[37] S. Amthor, B. Noller, C. Lambert, *Chem. Phys.* **2005**, *316*, 141–152.

[38] F. A. Neugebauer, S. Bamberger, W. R. Groh, *Chem. Ber.* **1975**, *108*, 2406–2415.

[39] H. van Willigen, *J. Am. Chem. Soc.* **1967**, *89*, 2229–2230.

[40] a) M. Mikuriya, H. Azuma, J. Sun, D. Yoshioka, M. Handa, *Chem. Lett.* **2002**, *31*, 608–609; b) D. Maspoch, D. Ruiz-Molina, K. Wurst, J. Vidal-Gancedo, C. Rovira, J. Veciana, *Dalton Trans.* **2004**, 1073–1082; c) D. Maspoch, D. Ruiz-Molina, K. Wurst, C. Rovira, J. Veciana, *Chem. Commun.* **2002**, 2958–2959.

[41] D. Takamatsu, K.-i. Fukui, S. Arouac, Y. Yamakoshi, *Org. Biomol. Chem.* **2010**, *8*, 3655–3664.

[42] S. Stoll, A. Schweiger, *J. Magn. Reson.* **2006**, *178*, 42–55.

[43] a) B. Nonius, in *COLLECT; Data Collection Software* Delft, The Netherlands, **1998**; b) Z. Otwinowski, W. Minor, in *Methods in Enzymology: Processing of X-ray Diffraction Data Collected in Oscillation Mode, Vol. 276*, Academic Press, **1997**, pp. 307–326; c) in *Bruker AXS Inc., Madison, Wisconsin, USA. SADABS 2.10*, **2002**.

[44] G. M. Sheldrick, *Acta Crystallogr.* **2015**, *C71*, 3–8.

[45] A. L. Spek, *Acta Crystallogr.* **2015**, *C71*, 9–18.

[46] H. Putz, K. Brandenburg, in *Diamond 4.2.2 - Crystal and Molecular Structure Visualization*, Kreuzherrenstr. 102, 53227 Bonn, Germany.

[47] O. V. Dolomanov, L. J. Bourhis, R. J. Gildea, J. A. K. Howard, H. Puschmann, *J. Appl. Crystallogr.* **2009**, *42*, 339–341.

[48] L. J. Farrugia, *J. Appl. Crystallogr.* **2012**, *45*, 849–854.

[49] a) E. J. Baerends, D. E. Ellis, P. Ros, *Chem. Phys.* **1973**, *2*, 41–51; b) B. I. Dunlap, J. W. D. Connolly, Sabin, *J. Chem. Phys.* **1979**, *71*, 3396–3402; c) C. van Alsenoy, *J. Comput. Chem.* **1988**, *9*, 620–626.

[50] a) J. P. Perdew, Y. Wang, *Phys. Rev. B* **1992**, *45*, 13244–13249; b) J. P. Perdew, K. Burke, M. Ernzerhof, *Phys. Rev. Lett.* **1996**, *77*, 3865–3868.

[51] F. Weigend, R. Ahlrichs, *Phys. Chem. Chem. Phys.* **2005**, *7*, 3297–3305.

[52] in *TURBOMOLE V6.6 2014, development of University of Karlsruhe and Forschungszentrum Karlsruhe GmbH, 1989–2007, TURBOMOLE GmbH, since 2007; available from http://www.turbomole.com.*

[53] J. P. Perdew, M. Ernzerhof, K. Burke, *J. Chem. Phys.* **1996**, *105*, 9982–9985.

[54] a) K. Yamaguchi, Y. Takahara, T. Fueno, in *Applied quantum chemistry*, Springer, **1986**, pp. 155–184; b) T. Soda, Y. Kitagawa, T. Onishi, Y. Takano, Y. Shigeta, H. Nagao, Y. Yoshioka, K. Yamaguchi, *Chem. Phys. Lett.* **2000**, *319*, 223–230.

Manuscript received: November 5, 2018
Revised manuscript received: December 2, 2018